Space Weather

RESEARCH ARTICLE
10.1029/2019SW002427

Interhemispheric Asymmetries in the Ground Magnetic Response to Interplanetary Shocks: The Role of Shock Impact Angle

Z. Xu[1,2], M. D. Hartinger[1,3], D. M. Oliveira[4,5], S. Coyle[1], C. R. Clauer[1], D. Weimer[1], and T. R. Edwards[6]

[1]Bradley Department of Electrical and Computer Engineering, Virginia Polytechnic Institute and State University, Blacksburg, VA, USA, [2]National Institute of Aerospace, Hampton, VA, USA, [3]Space Science Institute, Boulder, CO, USA, [4]Goddard Planetary Heliophysics Institute, University of Maryland, Baltimore County, Baltimore, MD, USA, [5]Geospace Physics Laboratory, NASA Goddard Space Flight Center, Greenbelt, MD, USA, [6]DTU Space, Technical University of Denmark, Kongens Lyngby, Denmark

Abstract Interplanetary (IP) shocks drive magnetosphere-ionosphere (MI) current systems that in turn are associated with ground magnetic perturbations. Recent work has shown that IP shock impact angle plays a significant role in controlling the subsequent geomagnetic activity and magnetic perturbations; for example, highly inclined shocks drive asymmetric MI responses due to interhemispherical asymmetric magnetospheric compressions, while almost head-on shocks drive more symmetric MI responses. However, there are few observations confirming that inclined shocks drive such asymmetries in the high-latitude ground magnetic response. We use data from a chain of Antarctic magnetometers, combined with magnetically conjugate stations on the west coast of Greenland, to test these model predictions (Oliveira & Raeder, 2015, https://doi.org/10.1002/2015JA021147; Oliveira, 2017, https://doi.org/10.1007/s13538-016-0472-x). We calculate the time derivative of the magnetic field ($\partial B/\partial t$) in each hemisphere separately. Next, we examine the ratio of Northern to Southern Hemisphere $\partial B/\partial t$ intensities and the time differences between the maximum $\partial B/\partial t$ immediately following the impact of IP shocks. We order these results according to shock impact angles obtained from a recently published database with over 500 events and discuss how shock impact angles affect north-south hemisphere asymmetries in the ground magnetic response. We find that the hemisphere the shock strikes first usually has (1) the first response in $\partial B/\partial t$ and (2) the most intense response in $\partial B/\partial t$. Additionally, we show that highly inclined shocks can generate high-latitude ground magnetic responses that differ significantly from predictions based on models that assume symmetric driving conditions.

Key Points:
- High latitude interhemispheric comparisons are performed to study asymmetries in ground magnetic perturbations caused by shock inclinations
- The hemisphere the shock strikes first usually has (1) the first response in $\partial B/\partial t$ and (2) the most intense response in $\partial B/\partial t$
- Impact angles are an important parameter controlling the timing and intensity of the ground magnetic response to interplanetary shocks

Correspondence to:
Z. Xu,
zxu77@vt.edu

Citation:
Xu, Z., Hartinger, M. D., Oliveira, D. M., Coyle, S., Clauer, C. R., Weimer, D. R., & Edwards, T. R. (2020). Interhemispheric asymmetries in the ground magnetic response to interplanetary shocks: The role of shock impact angle. *Space Weather*, *18*, e2019SW002427. https://doi.org/10.1029/2019SW002427

Received 10 DEC 2019
Accepted 27 FEB 2020
Accepted article online 28 FEB 2020

1. Introduction

Interplanetary (IP) shocks are a common phenomenon in the heliosphere (Burlaga, 1971; Richter et al., 1985). While being more frequent during solar maxima, IP shocks can also be found, though less numerous, in any other phase of the solar cycle, including solar minima, due to their connection to solar activity (e.g., Oh et al., 2007; Oliveira & Raeder, 2015; Rudd et al., 2019). IP shocks are formed in the interplanetary space when the relative velocity between the shock disturbance and the local environment is greater than the local magnetosonic speed (Burguess, 1995; Landau & Lifshitz, 1960; Oliveira, 2017; Richter et al., 1985). In addition to this condition, if shocks propagate away from the Sun in the interplanetary space, they are classified as fast forward shocks, the most geoeffective class of shocks. Usually, strengths of IP shocks are expressed by shock speeds and magnetosonic Mach numbers, defined as the ratio between the shock/medium relative velocity to the local magnetosonic speed (Burlaga, 1971; Oliveira, 2017; Richter et al., 1985). One of the first prompt effects of IP shock impacts on the magnetosphere are sharp jumps in the horizontal magnetic field perturbations known as positive sudden impulses, or SI^+, that can be measured anywhere on the planet (Araki, 1994; Oliveira & Samsonov, 2018; Rudd et al., 2019; Smith et al., 1986; Wang et al., 2006).

IP shock impact angles are defined as the angle shock normal vectors perform with the Sun-Earth line. Usually, nearly frontal shocks (small impact angles) are driven by coronal mass ejections, while highly inclined shocks (large impact angles) are driven by corotating interaction regions (see Figure 1 of Oliveira

& Samsonov, 2018, and references therein). Numerical simulations and observational data have shown that the geomagnetic activity following IP shock impacts depends closely on the shock normal direction (see the comprehensive review by Oliveira & Samsonov, 2018). Nearly frontal shock impacts are associated with quasi-symmetric magnetosphere response, whereas highly inclined shock impacts are associated with highly asymmetric magnetosphere responses with respect to timing and intensity (Badruddin et al., 2019; Guo et al., 2005; Oliveira & Raeder, 2014, 2015; Oliveira & Samsonov, 2018; Oliveira et al., 2016; Rudd et al., 2019; Samsonov, 2011; Samsonov et al., 2015; Selvakumaran et al., 2017; Shi et al., 2019; Takeuchi et al., 2002; Wang et al., 2006). In addition, the inclination angles of solar wind phase fronts have recently been shown to control the subsequent geomagnetic activity even during quiet (non-shocked) solar wind conditions (Cameron et al., 2019).

Fast forward IP shocks are associated with increases in solar wind dynamic pressure and other variations in solar wind parameters that affect magnetosphere-ionosphere (MI) current systems and wave activity (e.g., Oliveira & Samsonov, 2018; Tsurutani et al., 2011). These MI current systems couple to a variety of spatially and temporally varying ground magnetic perturbations. IP shock impacts have been shown to drive particularly intense current systems and ground magnetic perturbations. The temporal variations of such magnetic perturbations, hereafter referred to as "$\partial B/\partial t$", are of particular interest due to their relationship with geomagnetically induced currents, known as GICs (Pirjola, 2002; Viljanen, 1998). GICs generate electric fields that couple with artificial conductors, which in turn create the flow of undesirable electric currents in power systems, leading to equipment damage, overtime degradation, and disruption of power supplies (Albertson et al., 1993; Béland & Small, 2005; Kappenman, 2003; Marshall et al., 2012; Ngwira & Pulkkinen, 2019; Oliveira & Ngwira, 2017). GICs associated with IP shock impacts have been identified to occur at low, mid, and high latitudes as well (e.g., Béland & Small, 2005; Carter et al., 2015, 2016; Espinosa et al., 2019; Fiori et al., 2014; Kappenman, 2003; Oliveira et al., 2018; Zhang et al., 2015, 2016).

Numerical magnetohydrodynamic simulations of shock impacts conducted by Oliveira and Raeder (2014), with shock normals lying in the meridional plane with different inclinations, indicate significant north-south hemisphere asymmetries in magnetospheric magnetic perturbations. For example, Oliveira and Raeder (2014) showed that time delays between the propagation of magnetosonic waves in the Northern and Southern Hemispheres triggered by a highly inclined shock caused a highly asymmetric magnetosphere compression, leading to asymmetric magnetospheric response, and weaker/slower MI-coupling response. On the other hand, as pointed out by the authors, impacts of high-speed and nearly frontal shocks are usually associated with symmetric magnetospheric compressions that in turn amplify the subsequent MI response. These latter simulation results were confirmed by Shi et al. (2019), who used Active Magnetosphere and Planetary Electrodynamics Response Experiments to show that high-latitude field-aligned currents following nearly-frontal shock impacts responded faster and more strongly than those following highly inclined shock impacts. However, there is limited observational evidence to test the prediction that north-south inclined shocks drive north-south asymmetries in magnetospheric perturbations or ground-based $\partial B/\partial t$, particularly at high latitudes. Previous observational studies of high latitude north-south inter-hemispheric comparisons of $\partial B/\partial t$ related to shocks and/or upstream pressure variations found significant hemispheric asymmetries in $\partial B/\partial t$, yet could only examine the relationship between $\partial B/\partial t$ and factors such as ionospheric conductivity (season) or magnetic field topology due to a lack of information about shock impact angle (Hartinger et al., 2017).

In this work, we use a recently published database of shock impact angles from Oliveira et al. (2018), along with a recently deployed chain of magnetically conjugate ground magnetometers to test hypotheses motivated by the simulations of Oliveira and Raeder (2014), namely the hemisphere that the IP shock strikes first has (i) the first ground magnetic response; and (ii) the most intense response. These hypotheses are motivated by the fact that, at least initially, shocks ought to create disturbances on the dayside magnetopause that couple to magnetosonic and Alfvén waves. These waves have a shorter distance to travel to the ionosphere in one hemisphere if the shock first strikes the magnetopause closer to that hemisphere; thus, the waves may arrive sooner in that hemisphere, experience less dispersion, and potentially generate a larger initial ground magnetic perturbation. In other words, if a shock creates a magnetopause disturbance that exhibits an asymmetry with respect to the magnetic equator, one generally expects this disturbance to generate magnetospheric waves and corresponding ground magnetic perturbations that also exhibit north-south asymmetries because their energy source is asymmetric. The paper is structured as follows: section 2 presents the data and methodologies used in this study; section 3 presents case studies and

Table 1
The Coordinates of Ground Magnetometers Used in this Study

Station code	Geodetic LON	Geodetic LAT	MagLON IGRF2015	MagLAT IGRF2015	Station location
PG0	88.68	−83.67	38.01	−78.64	EAP[a]
PG1	77.20	−84.50	37.15	−77.24	EAP
PG2	57.96	−84.42	38.95	−75.53	EAP
PG3	37.63	−84.81	36.56	−73.79	EAP
PG4	12.25	−83.34	36.27	−71.05	EAP
PG5	5.71	−81.96	37.16	−69.65	EAP
THL	290.77	77.47	26.79	84.05	WCG[b]
TAB	291.18	76.54	25.25	83.19	WCG
SVS	294.90	76.02	30.73	82.31	WCG
KUV	302.82	74.57	39.83	79.98	WCG
UPN	303.85	72.78	38.49	78.18	WCG
UMQ	307.87	70.68	41.07	75.59	WCG
GDH	306.47	69.25	38.10	74.42	WCG
ATU	306.43	67.93	37.05	73.14	WCG
STF	309.28	67.02	39.74	71.77	WCG
SKT	307.10	65.42	36.29	70.54	WCG
GHB	308.27	64.17	36.99	69.07	WCG
FHB	310.32	62.00	38.29	66.47	WCG
NAQ	314.56	61.16	42.37	64.78	WCG

[a]East Antarctic Plateau. [b]West Coast of Greenland.

statistics of hemispheric comparisons of the ground magnetic response during inclined and frontal shocks; section 4 discusses these results and their implications, and section 5 summarizes the results.

2. Data and Methodology

2.1. IP Shock Dataset

We use the IP shock list found in the supporting information of Oliveira et al. (2018) in our analysis. This list contains 547 fast forward shocks from January 1995 to September 2017. Solar wind plasma and interplanetary magnetic field data obtained from the Advanced Composition Explorer and Wind spacecraft located in the solar wind at L1 upstream of the Earth were used to compute shock normal inclination angles and speeds. Assumptions of energy and momentum conservation across the shock fronts were used along with the Rankine-Hugoniot conditions during the calculations (e.g., Burlaga, 1971; Landau & Lifshitz, 1960). The theoretical framework and the equations particularly used in these calculations can be found in many previous papers (Oliveira & Raeder, 2014, 2015; Oliveira et al., 2016; Oliveira, 2017; Oliveira & Samsonov, 2018). A recent and detailed statistical analysis of the events in this shock list has been provided by Rudd et al. (2019).

2.2. High-latitude Ground Magnetometer Datasets

For this work, we use data from two ground magnetometer chains, one on the west coast of Greenland operated by the Technical University of Denmark (DTU, https://www.space.dtu.dk/English/Research/Scientific&urluscore;data&urluscore;and&urluscore;models/Magnetic&urluscore;Ground&urluscore;Stations.aspx) and the other on the East Antarctic Plateau operated by Virginia Tech, named Autonomous Adaptive Low-Power Instrument Platforms (AAL-PIP, Clauer et al., 2014). DTU data are obtained from the public Tromsø Geophysical Observatory website (http://flux.phys.uit.no/geomag.html), while AAL-PIP data are obtained from the public Magnetosphere-Ionosphere Science Team (MIST) website (mist.nianet.org). AAL-PIP data have been used to investigate interhemispheric asymmetries in ground- and space-located magnetic perturbations (Hartinger et al., 2016, 2017; Martines-Bedenko et al., 2018; Xu et al., 2017).

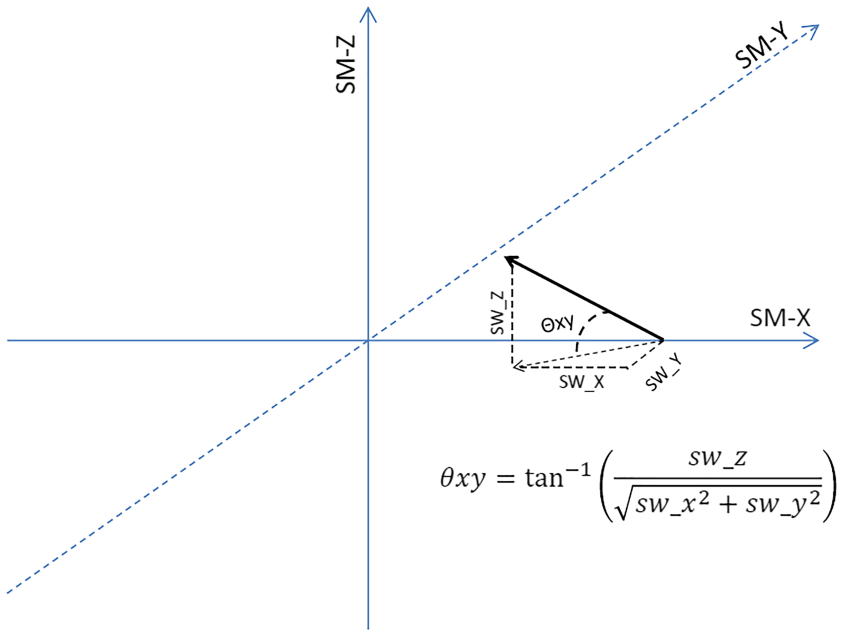

Figure 1. Illustration of θ_{xy}, the angle between the shock normal and the solar magnetic (SM) xy plane (dipole equator). sw_x, sw_y, and sw_z stand for the normal X, Y, and Z of interplanetary shock normals in SM coordinates accordingly.

By design, the AAL-PIP stations were placed at the magnetic conjugate points of the DTU stations, as determined through use of the International Geomagnetic Reference Field (IGRF). The geographic and magnetic coordinates of these stations are listed in Table 1. The AAL-PIP and DTU data are both in sensor coordinates roughly equivalent to NEZ coordinates, defined as N = magnetic north, Z = vertical (towards Earth), E = completes right-hand orthogonal set and points roughly eastward. The units of all components are nT. In the present study, we only analyze the N component because it is more susceptible and consequently the most important component to magnetospheric forcing (e.g., Ngwira et al., 2009).

For this study, we require shock normal angles in solar magnetic (SM) coordinates; we choose to use SM coordinates because the magnetometer station locations are organized according to the Earth's magnetic field; thus, interhemispheric comparisons will be more meaningful in this coordinate system (Laundal & Richmond, 2016). We thus obtained the shock normal vectors in geocentric solar ecliptic (GSE) coordinates from the IP shocks in Oliveira et al. (2018) and used these vectors to compute the angle between the shock normal and the SM xy plane, or θ_{xy}:

$$\theta_{xy} = tan^{-1}\left(\frac{sw_z}{\sqrt{sw_x{}^2 + sw_y{}^2}}\right) \quad (1)$$

where sw_x, sw_y, and sw_z are the x, y, and z components of the shock normal in SM coordinates. This angle is illustrated in Figure 1. Nearly frontal shocks correspond to small angles while highly inclined shocks have larger angles. Recall that the shock front is in a plane orthogonal to the shock normal. Thus, positive angles indicate the Southern Hemisphere will be struck by the shock front first, while negative angles indicate the northern hemisphere will be struck first. We organize data in SM coordinates rather than GSE (as in Oliveira & Samsonov, 2018) because, as noted above, the ground station locations in each hemisphere are ordered by the Earth's magnetic field.

2.3. Signal Processing and Data Reduction

For this study, we focus exclusively on the analysis of the N component. For statistical analysis, we use data from a single north-south station pair, UMQ-PG1 because PG1 was deployed in 2008 – far earlier than the other stations – thus it enables analysis of significantly more shock events for more robust statistical results, as shown in Table 2 for data reduction. For case study analysis, we use all available stations.

Table 2
Data Reduction for Statistical Analysis of Interplanetary (IP) Shocks Using UMQ-PG1

Data Analysis Step	Number of events
All events in Oliveira et al. (2018)	547
From May 2009 to Sept. 2017	169
With high quality data from PG1[a]	143
With high quality data from UMQ[a]	150
With high quality data from both[a]	127
High quality from both, dayside events[a]	65
High quality from both, nightside events[a]	62
High quality from both, $\theta_{xy} > 20°$ [a]	90
High quality from both, $\theta_{xy} > 20°$, dayside events[a]	49
High quality from both, $\theta_{xy} > 20°$, nightside events[a]	41

[a]After 2009.

Before analyzing $\partial B/\partial t$ related to IP shocks, we perform several signal processing steps:

1. Despike the raw 10 s DTU magnetometer and 1 s PG magnetometer data.
2. For consistency and ease of comparison with Oliveira et al. (2018), the time series from both arrays are averaged to 1 minute samples.
3. Remove background trends from a 1 minute time series by subtracting an average value for each station for the day when the shock occurred; then, since the data have uniform time resolution, we directly obtain $\partial B/\partial t$. Examples of these data are shown in Figures 2 and 3.
4. We extract the time and intensity of the largest $\partial B/\partial t$ in the N component in a 25 minute window surrounding the shock time (5 minutes before shock to 20 minutes after), similar to Oliveira et al. (2018).

We statistically analyze the relationship between θ_{xy} and two parameters: (1) time lag between the first response in the north versus the south, (2) intensity ratio between the maximum $\partial B/\partial t$ measured in the north and the south. We require simultaneous measurements at conjugate station pairs to obtain these quantities, and we also require a large number of IP shock events to obtain robust statistical results. We thus limit our statistical analysis to the PG1-UMQ station pair because PG1 was deployed earlier than the other PG stations (2008), significantly increasing the number of IP shock events available for analysis. Table 2 shows how our requirements limit the number of events for analysis, yet it also shows that there are sufficient events available to test the two hypotheses presented in section 1. For our statistical analysis, we analyze periods when data are available and are of high quality – no large spikes or gaps – from both PG1 and UMQ. To test our hypotheses, we focus exclusively on inclined shocks ($\theta_{xy} > 20$ degrees). We also analyze event subsets corresponding to periods when PG1-UMQ are at dayside and nightside local times.

3. Results

3.1. Case Study Comparison

We first use a case study comparison to explore the effects of shock impact angles on ground magnetometer response and whether the hemisphere that the IP shock strikes first has the first and/or the most intense ground magnetic response. We selected events meeting the following criteria: (i) occur at similar UTs to reduce complicating factors such as spatially varying current systems, and (ii) similar shock speeds and magnetosonic Mach numbers (M_s) because shock strength is an important parameter controlling ground response that would bias this analysis (Oliveira & Samsonov, 2018). The parameters for the shock events we selected are shown in Table 3. The shock impact angles indicate that the highly inclined shock will strike the Northern Hemisphere first, while the nearly frontal shock case will strike both hemispheres at roughly the same time. Finally, we note that due to a limited number of shock events, we could not identify two shock events with identical properties apart from shock impact angle. As a result, other factors such as ionospheric conductivity (events occurred at different times of the year) and shock compression ratio may affect the intensity of the ground magnetic response. We return to this point later in this section and in section 4, but for now we simply note that these case studies will only be used to illustrate the potential dependence of ground magnetic perturbation intensity/arrival time on the shock impact angle.

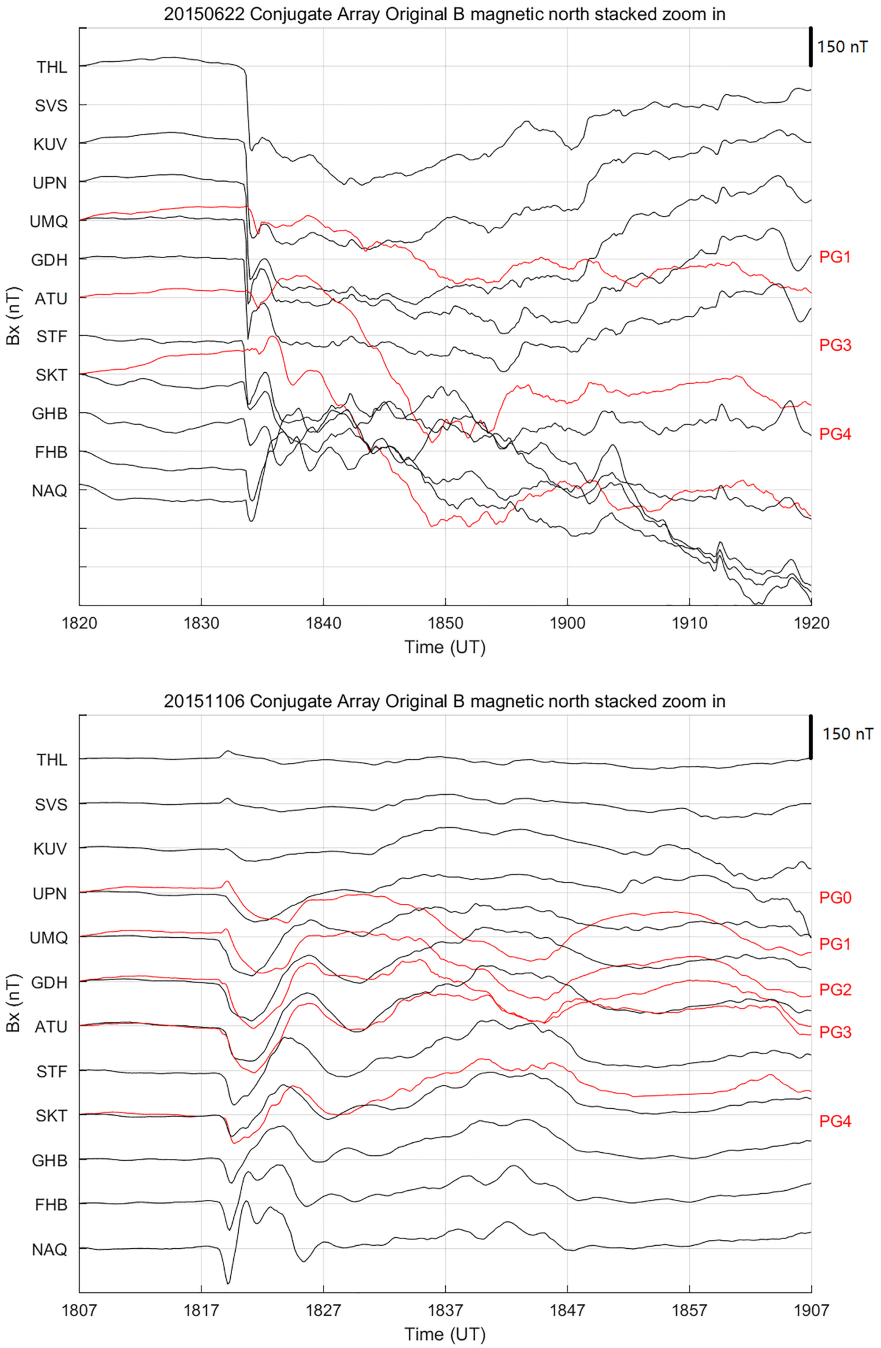

Figure 2. (Top) N component of the magnetic perturbations at different Northern Hemisphere (black lines) and Southern Hemisphere (red lines) stations for the highly inclined shock case. Each division on the *y*-axis corresponds to 150 nT. (Bottom) The same, but for the nearly frontal shock case.

The upper part of Figure 2 shows a 1 hour time range for the highly inclined shock case on 22 June 2015, while the lower part of Figure 2 is the same for the nearly frontal shock case. The stack plot shows signals (magnetic perturbation of N component) measured from northern (black lines) and southern (red lines) hemisphere stations ordered according to magnetic latitude (closest to respective poles at the top). The ground magnetic response in the two hemispheres is generally different in the inclined shock case (compare red to black curves in top panel), whereas in the frontal shock case it is generally similar. Moreover, in the inclined shock case significant negative deflections occur at much higher latitudes than in the frontal shock case, and those deflections are much more intense in the Northern Hemisphere; for example, the

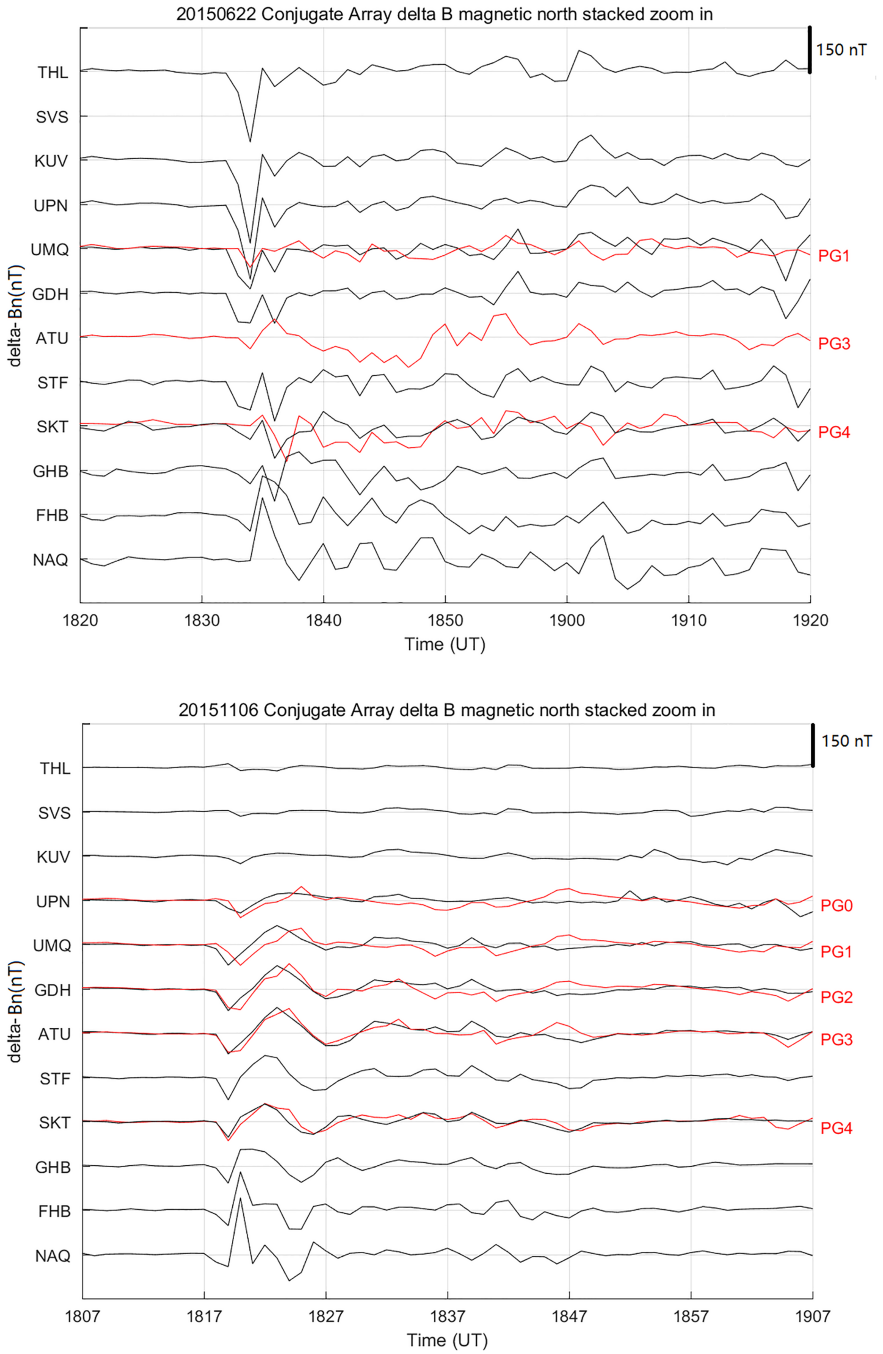

Figure 3. (Top) N component of $\partial B/\partial t$ variations observed at different Northern Hemisphere (black lines) and Southern Hemisphere (red lines) stations for the highly inclined shock case. Each division on the y-axis corresponds to 150 nT. (Bottom) The same, but for the nearly frontal shock case.

perturbation at UMQ is more than double that at PG1. In comparison, the magnetic perturbations for the frontal shock case are very similar in amplitude and timing (red and black curves in bottom panel lie almost on top of each other).

Figure 3 is in the same format as Figure 2, but it shows $\partial B/\partial t$ variations rather than magnetic perturbations. When comparing the top part of Figure 3 (inclined shock) to the bottom part (frontal shock), one of the most striking differences is the north-south hemisphere asymmetries present in the inclined shock case but not in the frontal shock case. In particular, the red and black curves on the top often behave differently, while on the bottom they lie on top of each other indicating symmetric behavior. There is a clear SI signature in the

Table 3
Interplanetary (IP) Shock Parameters for Case Study Comparison

Shock normal inclination	Date	UT	Shock speed	M_s	P_{up}/P_{down}	θ_{xy} in SM
Highly inclined shock	2015-06-22	1833	800.81 km/s	4.13	8.11	−42.08°
Nearly frontal shock	2015-11-06	1819	747.94 km/s	4.75	1.76	1.53°

frontal case, in PG0 and PG1 station. But there is no SI signature in the northern hemisphere. Examining the UMQ-PG1 pair on the top, the time with the largest $\partial B/\partial t$ value occurs later in the Southern Hemisphere (PG1, red) compared with the Northern Hemisphere (UMQ, black), consistent with the shock striking the Northern Hemisphere first. The intensity of the maximum $\partial B/\partial t$ is also larger in the north compared to the south.

These case studies are consistent with our hypothesis that the hemisphere the shock strikes first has the first response in $\partial B/\partial t$: in the inclined shock case with negative impact angle the Northern Hemisphere generally sees an earlier response than the Southern (features of black curves shifted slightly right of red), while in the frontal shock case the red and black curves are nearly on top of each other consistent with a similar arrival time in each hemisphere. They are also generally consistent with the second hypothesis that the hemisphere the shock strikes first has the most intense response: the Northern Hemisphere has a more intense response than the southern in the inclined shock case at the PG1-UMQ station pair (or they are comparable, as in PG4-SKT case), while in the frontal shock case the intensities are the same at all pairs (red and black curves lie nearly on top of each other). We examine whether these two hypotheses are consistent with other shock events in sections 3.2 and 3.3.

Finally, we note from Figure 3 that at many latitudes, particularly in the Southern Hemisphere, the frontal shock (bottom panel) generates comparable or more intense $\partial B/\partial t$ than the inclined shock (upper panel); this is consistent with the results of Oliveira et al. (2018). However, this pattern does not hold at all latitudes; in particular, the inclined shock generates magnetic perturbations with significantly larger intensities than the frontal shock at many latitudes in the Northern Hemisphere. We would expect a stronger trend towards larger $\partial B/\partial t$ for the frontal shock if the shock speeds, magnetosonic Mach numbers, and upstream/downstream dynamic pressure ratios were equal, but the pressure ratio is more than 4 times larger in the inclined shock case, as shown in Table 3, leading to the larger magnetic intensities in the inclined shock event.

3.2. Statistical Analysis of PG1-UMQ: Time Lag of First Response

Now we statistically investigate the effects of shock inclinations on our first hypothesis. Figure 4 shows results for inclined shock events that satisfy the condition $\theta_{xy} > 20°$, where both UMQ and PG1 had data. The blue bars indicate results for all events. Events are organized according to categories related to the shock impact angle and the hemisphere where the response in $\partial B/\partial t$ was first observed following the arrival of the shock. "First response in hemisphere shock strikes first" is for the case when the shock front strikes the hemisphere first and the hemisphere station observes the first response. "First response in the opposite hemisphere from where shock strikes first" is for the case when the shock front strikes the one hemisphere first but the station in the opposite hemisphere observes the first response. A third category, not shown in the plot, is for events where the response occurred simultaneously in both hemispheres, to within the 1 minute sampling rate; these events are excluded from the analysis because no conclusion can be drawn concerning time lag; however, we note these events are a minority, 15 cases over 90 cases total. The blue, red, and green bars at the left edge of the histogram plot are consistent with our time lag hypothesis, while those on the right are not; in other words, if our hypothesis is correct there should be more events in the "First response in hemisphere shock strikes first" category compared with the "First response in the opposite hemisphere from where shock strikes first" category. This is indeed the case.

The red and green bars in Figure 4 further separate inclined shock events according to the local time of the ground stations when the shock first arrives. These results indicate that whether the stations are on the dayside or the nightside, the trend is generally the same.

3.3. Statistical Analysis of PG1-UMQ: North-South $\partial B/\partial t$ Ratio

In order to address our second hypothesis, we examine Figure 5 for inclined shock events ($\theta_{xy} > 20$ degrees) where both UMQ and PG1 had data. Blue bars show results for all events, while red and green bars are

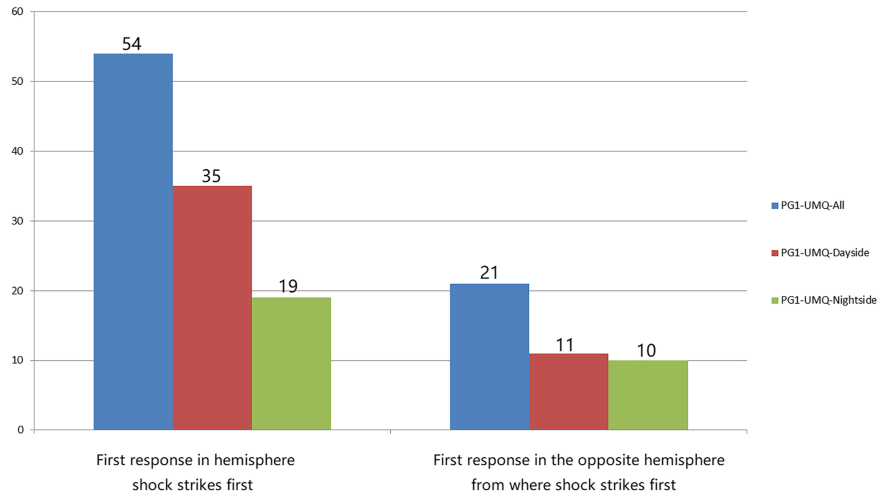

Figure 4. Histogram plot showing inclined shock events sorted as: "First response in hemisphere shock strikes first" when the shock strikes one hemisphere first and the first $\partial B/\partial t$ response is observed in the same hemisphere and "First response in the opposite hemisphere from where shock strikes first" when the shock strikes one hemisphere first and the first response is observed in the opposite hemisphere. Blue bars include all inclined shock events; red bars indicate only events that occurred when the PG1 station was on the dayside; green bars indicate events on the nightside. Note events were not included in this plot when the time of arrival was the same (within 1 minute). The number of events in each group is shown above its corresponding bar.

for dayside and nightside events, respectively, as in Figure 4. Events are organized according to categories related to the shock impact angle and the hemisphere where the most intense $\partial B/\partial t$ was observed following the arrival of the shock. "Most intense response in hemisphere shock strikes first" is for the case when the shock front strikes one hemisphere first and the station in the same hemisphere observes the most intense $\partial B/\partial t$, and "Most intense response in the opposite hemisphere from where shock strikes first" is for the case when the shock front strikes one hemisphere first but the station in the opposite hemisphere observes the most intense response. A third category, not shown in the plot, is for events where the response

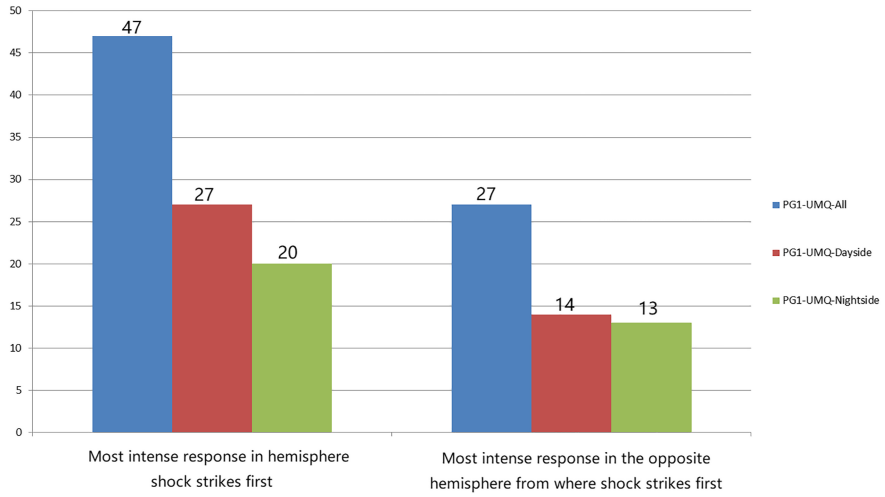

Figure 5. Histogram plot showing interplanetary shock events sorted as "Most intense response in hemisphere shock strikes first" when the shock strikes one hemisphere first and the most intense $\partial B/\partial t$ response is observed in the same hemisphere and "Most intense response in the opposite hemisphere from where shock strikes first" when the shock strikes one hemisphere first and most intense response is observed in the opposite hemisphere. Blue bars include all interplanetary shock events, red bars indicate only events that occurred when the PG1 station was on the dayside, green bars indicate events on the nightside. Note events were not included in this plot when the intensities in each hemisphere were similar (within 5%). The number of events in each group is shown above its corresponding bar.

had the same intensity, to within 5%, in both hemispheres. These events are not included in the analysis because no conclusion can be drawn concerning intensity differences (16 cases over 90 cases total).

The blue, red, and green bars at the left of the histogram plot (Figure 5) are consistent with our intensity hypothesis. In other words, if our hypothesis is correct there should be more events in the "Most intense response in hemisphere shock strikes first" category compared with the "Most intense response in the opposite hemisphere from where shock strikes first" category. This trend is confirmed: the most intense $\partial B/\partial t$ response is most often observed in the hemisphere where the shock strikes first.

Examining subcategories for specific local times, the trend also generally holds.

4. Discussion

In the previous section, we used a chain of magnetically conjugate ground magnetometer stations to test the hypotheses that the hemisphere an IP shock strikes first has (i) the first ground magnetic response; and (ii) the most intense response. These hypotheses were motivated by the numerical simulations of Oliveira and Raeder (2014) and the fact that shocks ought to create disturbances on the dayside magnetopause that couple to magnetosonic and Alfvén waves. These waves have a shorter distance to travel to the ionosphere in one hemisphere if the shock first strikes the magnetopause closer to that hemisphere, thus the waves may arrive sooner in that hemisphere, experience less dispersion, and potentially generate a larger initial ground magnetic perturbation.

Figure 4 is consistent with our first hypothesis: the hemisphere that the shock strikes first has the first response in $\partial B/\partial t$ (more events in "First response in hemisphere shock strikes first" categories compared to "First response in the opposite hemisphere from where shock strikes first"). This is true regardless of the local time of the station. Figure 5 is consistent with our second hypothesis: the hemisphere that the shock strikes first has the most intense response in $\partial B/\partial t$. This is also true regardless of the local time of the station. Taken together, both Figures are consistent with the numerical simulations of Oliveira and Raeder (2014) showing that shock normals lying in the meridional plane with large inclinations create significant north-south hemisphere asymmetries in magnetospheric magnetic perturbations. Their simulations indicated north-south hemisphere time delays in the propagation of magnetosonic waves, highly asymmetric magnetospheric compression, and asymmetric MI-coupling responses during highly inclined shock events. The authors noted that such asymmetries ought to be evident at all magnetic latitudes. The present study observationally confirms that such asymmetries occur at high latitudes.

As can be seen in both Figures 4 and 5, shock impact angle is not the only factor controlling north-south hemisphere asymmetries in timing and intensity; several events fall into "first-opposite" categories, meaning the first response and/or most intense response in $\partial B/\partial t$ occurred in the hemisphere opposite from the shock's first arrival. There are several factors that could potentially explain these events. For example, the arrival time is affected by magnetospheric wave speeds (e.g., Chi et al., 2006) that vary from event to event and may themselves be asymmetric with respect to the dipole equator. As another example, the intensity of the initial ground magnetic response depends on ionospheric conductivity and should have a seasonal dependence due to the seasonal dependence on solar extreme ultraviolet (EUV)/conductivity (Equation 10 in Pilipenko et al., 2020), perhaps leading to a seasonal dependence in the magnetic intensity ratio; this contributed at least in part to the intensity asymmetries seen in Figures 2 and 3, though it cannot explain the extremely symmetrical response seen in the frontal shock event as this event occurred near solstice when there should have been larger asymmetries (if conductivity was the primary factor controlling the asymmetry in this event).

Additionally, other interplanetary magnetic field (IMF) and solar wind parameters may affect this shock response, such as IMF strength (Meurant et al., 2004), magnetopheric precondition determined by IMF B_z (Yue & Zong, 2011; Zhou & Tsurutani, 2001), and solar wind dynamic pressure enhancements (Chua et al., 2001). Even in the absence of shocks, Maynard et al. (2001) showed that ground-based optical data are well ordered by considering that incoming solar wind phase fronts are tilted, allowing different hemispheres to respond at different times due to differences in merging location. More generally, it has been known for quite a while that the northern and southern hemispheres have different responses to the Y component of the IMF regardless of the presence of a shock (e.g., Friis-Christensen & Wilhjelm, 1975; Haaland et al., 2007). Though an investigation of all these factors is outside the scope of the present study, future work should

examine the interplay between IP shock parameters and other factors that are known to control large scale current systems driven by shocks, such as magnetospheric plasma conditions and ionospheric conductivity.

We have excluded nearly frontal shocks ($\theta_{xy} < 20$ degrees) from our analysis in Figures 4 and 5 in order to test whether inclined shocks drive north-south hemisphere asymmetries. For brevity, we do not show the results for frontal shocks here, but we note that the trends seen in Figures 4 and 5 becoming much weaker or nonexistent when frontal shocks are considered. This is also consistent with Oliveira and Raeder (2014), who showed that nearly frontal shocks create symmetric MI-coupling responses.

Our statistical analysis in Figures 4 and 5 only examined one north-south hemisphere station pair (magnetic latitude), UMQ-PG1, and one aspect of the MI-coupling response to highly inclined shocks: the maximum $\partial B/\partial t$ immediately following the shock. Our case study results examining a wider range of latitudes indicate that significantly more work is needed to understand the complex high-latitude response to inclined shocks. As can be seen in Figures 2 and 3, highly inclined shocks can drive a dramatically different ground magnetic response when compared with frontal shocks; the frontal shock case (lower panel of both figures) is consistent with expectations from past observational and modeling studies (e.g., compare bipolar response on right of Figure 2 to Figure 11b in Araki, 1994), while the inclined shock case has step-like changes, intense magnetic perturbations and $\partial B/\partial t$ extending to very high latitudes in the Northern Hemisphere, and, overall, significant hemispheric differences in the spatial and temporal dependence of the ground magnetic response to the shock. More observational and modeling work is needed to understand these differences.

Our results have important implications for future work seeking to model and predict $\partial B/\partial t$ at high latitudes: the impact angle of shocks must be considered to fully characterize the MI-coupling response and $\partial B/\partial t$ related to shocks. This conclusion is consistent with Oliveira et al. (2018), who found that $\partial B/\partial t$ at a wide range of latitudes depends on the shock impact angle. Our results indicate that ignoring the shock impact angle in model predictions of ground magnetic perturbations – for example, explicitly or implicitly setting θ_{xy} to 0 in a global MHD simulation of a highly inclined shock event – would significantly alter the resulting ground magnetic response and $\partial B/\partial t$ in each hemisphere, changing it from the highly asymmetric response seen on the upper part of Figure 2 to a symmetric response more like the right part of Figure 2.

Finally, the results of this work are relevant not only to numerical simulation studies to provide more realistic results, but also to studies focused on forecasting and prediction of GICs. This is primarily indicated by the previous knowledge of meridional angles of IP shock normals that determine which magnetosphere hemisphere the shock impacts first. As a result, predicting and forecasting which hemisphere will be impacted first and which hemisphere will most likely have the highest $\partial B/\partial t$ response may provide opportunities to prevent overtime degradation of power transmission line equipment. Therefore, the shock impact angle is indeed an important factor for GIC research, as previously pointed out by Oliveira et al. (2018).

5. Summary

We used a recently published database of shock impact angles from Oliveira et al. (2018), along with a recently deployed chain of magnetically conjugate ground magnetometers to test hypotheses motivated by the simulations of Oliveira and Raeder (2014), namely the hemisphere that the IP shock strikes first has (i) the first ground magnetic response and (ii) the most intense response. We find that the hemisphere the shock strikes first generally has the first response in $\partial B/\partial t$ and the most intense, though other factors such as the local time dependence of the M-I current systems excited by the shock and the ionosphere conductivity play important roles.

In this work, we only examined the first response in $\partial B/\partial t$ following the arrival of the shock. As shown in the case studies in section 3.1 and numerous past publications, IP shocks excite a wide variety of magnetospheric current systems and wave activity, and the properties of these currents/waves may be more sensitive to the shock impact angle as shown, for example, in the wave activity simulated by Oliveira and Raeder (2014). The highly inclined shock case examined here indicates that significantly more work is needed to understand the high latitude ground magnetic response to such shocks, as this response deviates significantly from model predictions (see section 4). The role of shock impact angle in affecting other currents/waves is an important topic for future work, in addition to more research needed to understand general shock impact angle effects on GICs generated in a wide range of latitude regions.

Acknowledgments
Z. Xu and M.D. Hartinger were supported by NSF1543364 and 1744828. D.M. Oliveira acknowledges the NASA Grant HISFM18-HIF (Heliophysics Innovation Fund). All data used in the analysis are publicly available at the following repositories: AALPIP magnetometer at mist.nianet.org or NASA CDAWeb, DTU 10s Greenland magnetometer data the Tromso Geophysical Observatory at http://flux.phys.uit.no/geomag.html. The shock database is available in the supporting information of publications cited in the text.

References

Albertson, V. D., Bozoki, B., Feero, W. E., Kappenman, J. G., Larsen, E. V., Nordell, D., et al. (1993). Geomagnetic disturbance effects on power systems. *IEEE Transactions on Power Delivery*, *8*(3), 1206–1216.

Araki, T. (1994). A physical model of the geomagnetic sudden commencement. In M. J. Engebretson, K. Takahashi, & M. Scholer (Eds.), *Solar wind sources of magnetospheric ultra-low-frequency waves, Geophysical Monograph Series* (Vol. 81, pp. 183–200). Washington, DC: American Geophysical Union.

Badruddin, Kumar, A., & Derouich, M. (2019). Study of the travelling interplanetary shocks, their earth crossings and resulting geomagnetic disturbances. *Astrophysics and Space Science*, *364*(4), 1–8.

Béland, J., & Small, K. (2005). Space weather effects on power transmission systems: The cases of hydro-Québec and Transpower New Zealand Ltd. In I. A. Daglis (Ed.), *Effects of space weather on technology infrastructure* (pp. 287–299). Dordrecht, The Netherlands: Springer.

Burguess, D. (1995). Collisionless shocks. In M. G. Kivelson & C. T. Russell (Eds.), *Introduction to space plasma physics.* Cambridge, United Kingdom: Cambridge University Press.

Burlaga, L. F. (1971). Hydromagnetic waves and discontinuities in the solar wind. *Space Science Reviews*, *12*(5), 600–657.

Cameron, T. G., Jackel, B. J., & Oliveira, D. M. (2019). Using mutual information to investigate geoeffectiveness of solar wind phase fronts with different front orientations. *Journal of Geophysical Research: Space Physics*, *124*, 1582–1592. https://doi.org/10.1029/2018JA026080

Carter, B. A., Yizengaw, E., Pradipta, R., Halford, A. J., Norman, R., & Zhang, K. (2015). Interplanetary shocks and the resulting geomagnetically induced currents at the equator. *Geophysical Research Letters*, *42*, 6554–6559. https://doi.org/10.1002/2015GL065060

Carter, B. A., Yizengaw, E., Pradipta, R., Weygand, J. M., Piersanti, M., Pulkkinen, A., et al. (2016). Geomagnetically induced currents around the world during the March 17, 2015 storm. *Journal of Geophysical Research: Space Physics*, *121*, 10,496–10,507. https://doi.org/10.1002/2016JA023344

Chi, P. J., Lee, D.-H., & Russell, C. T. (2006). Tamao travel time of sudden impulses and its relationship to ionospheric convection vortices. *Journal of Geophysical Research*, *111*, A08205. https://doi.org/10.1029/2005JA011578

Chua, D., Parks, G., Brittnacher, M., Peria, W., Germany, G., Spann, J., & Carlson, C. (2001). Energy characteristics of auroral electron precipitation: A comparison of substorms and pressure pulse related auroral activity. *Journal of Geophysical Research*, *106*(A4), 5945–5956.

Clauer, C. R., Kim, H., Deshpande, K., Xu, Z., Weimer, D., Musko, S., et al. (2014). An autonomous adaptive low-power instrument platform (AAL-PIP) for remote high-latitude geospace data collection. *Geoscientific Instrumentation, Methods and Data Systems*, *3*, 211–227.

Espinosa, K. V., Padilha, A. L., & Alves, L. R. (2019). Effects of ionospheric conductivity and ground conductance on geomagnetically induced currents during geomagnetic storms: case studies at low-latitude and equatorial regions. *Space Weather*, *17*, 252–268. https://doi.org/10.1029/2018SW002094

Fiori, R. A. D., Boteler, D. H., & Gillies, D. M. (2014). Assessment of GIC risk due to geomagnetic sudden commencements and identification of the current systems responsible. *Space Weather*, *12*, 76–91. https://doi.org/10.1002/2013SW000967

Friis-Christensen, E., & Wilhjelm, J. (1975). Polar cap currents for different directions of the interplanetary magnetic field in the Y-Z plane. *Journal of Geophysical Research*, *80*(10), 1248.

Guo, X.-C., Hu, Y.-Q., & Wang, C. (2005). Earth's magnetosphere impinged by interplanetary shocks of different orientations. *Chinese Physics Letters*, *22*(12), 3221–3224.

Haaland, S. E., Paschmann, G., Förster, M., Quinn, J. M., Torbert, R. B., McIlwain, C. E., et al. (2007). High-latitude plasma convection from Cluster EDI measurements: Method and IMF-dependence. *Annales Geophysicae*, *25*(1), 239–253.

Hartinger, M. D., Clauer, C. R., & Xu, Z. (2016). Space weather from a southern point of view. Eos Transactions AGU 97.

Hartinger, M. D., Xu, Z., Clauer, C. R., Yu, Y., Weimer, D. R., Kim, H., et al. (2017). Associating ground magnetometer observations with current or voltage generators. *Journal of Geophysical Research: Space Physics*, *122*, 7130–7141. https://doi.org/10.1002/2017JA024140

Kappenman, J. G. (2003). Storm sudden commencement events and the associated geomagnetically induced current risks to ground-based systems at low-latitude and midlatitude locations. *Space Weather*, *1*(3), 1016.

Landau, L. D., & Lifshitz, E. M. (1960). *Electrodynamics of continuous media*. Oxford, England: Pergamon Press.

Laundal, K. M., & Richmond, A. D. (2016). Magnetic coordinate systems. *Space Science Reviews*, *206*(1-4), 1–33.

Marshall, R. A., Dalzell, M., Waters, C. L., Goldthorpe, P., & Smith, E. A. (2012). Geomagnetically induced currents in the New Zealand power network. *Space Weather*, *10*, S08003. https://doi.org/10.1029/2012SW000806

Martines-Bedenko, V. A., Pilipenko, V. A., Hartinger, M. D., Engebretson, M. J., Lorentzen, D. A., & Willer, A. N. (2018). Correspondence between the latitudinal ULF wave power distribution and auroral oval in conjugate ionospheres. *Sun and Geosphere*, *13*(1), 41–47.

Maynard, N. C., Burke, W. J., Sandholt, P. E., Moen, J., Ober, D. M., Lester, M., et al. (2001). Observations of simultaneous effects of merging in both hemispheres. *Journal of Geophysical Research*, *106*(A11), 24,551–24,578.

Meurant, M., Gérard, J.-C., Blockx, C., Hubert, B., & Coumans, V. (2004). Propagation of electron and proton shock-induced aurora and the role of the interplanetary magnetic field and solar wind. *Journal of Geophysical Research*, *109*, A10210. https://doi.org/10.1029/2004JA010453

Ngwira, C. M., McKinnell, L.-A., Cilliers, P. J., Viljanen, A., & Pirjola, R. (2009). Limitations of the modeling of geomagnetically induced currents in the South African power network. *Space Weather*, *7*, S10002. https://doi.org/10.1029/2009SW000478

Ngwira, C. M., & Pulkkinen, A. (2019). An introduction to geomagnetically induced currents. In J. L. Gannon, A. Swidinsky, & Z. Xu (Eds.), *Geomagnetically induced currents from the sun to the power grid* (pp. 3–13). Washington, DC: American Geophysical Union.

Oh, S. Y., Yi, Y., & Kim, Y. H. (2007). Solar cycle variation of the interplanetary forward shock drivers observed at 1 AU. *Solar Physics*, *245*(2), 391–410.

Oliveira, D. M. (2017). Magnetohydrodynamic shocks in the interplanetary space: A theoretical review. *Brazilian Journal of Physics*, *47*(1), 81–95. https://doi.org/10.1007/s13538-016-0472-x

Oliveira, D. M., Arel, D., Raeder, J., Zesta, E., Ngwira, C. M., Carter, B. A., et al. (2018). Geomagnetically induced currents caused by interplanetary shocks with different impact angles and speeds. *Space Weather*, *16*, 636–647. https://doi.org/10.1029/2018SW001880

Oliveira, D. M., & Ngwira, C. M. (2017). Geomagnetically induced currents: Principles. *Brazilian Journal of Physics*, *47*(5), 552–560.

Oliveira, D. M., & Raeder, J. (2014). Impact angle control of interplanetary shock geoeffectiveness. *Journal of Geophysical Research: Space Physics*, *119*, 8188–8201. https://doi.org/10.1002/2014JA020275

Oliveira, D. M., & Raeder, J. (2015). Impact angle control of interplanetary shock geoeffectiveness: A statistical study. *Journal of Geophysical Research: Space Physics*, *120*, 4313–4323. https://doi.org/10.1002/2015JA021147

Oliveira, D. M., Raeder, J., Tsurutani, B. T., & Gjerloev, J. W. (2016). Effects of interplanetary shock inclinations on nightside auroral power intensity. *Brazilian Journal of Physics*, *46*(1), 97–104.

Oliveira, D. M., & Samsonov, A. A. (2018). Geoeffectiveness of interplanetary shocks controlled by impact angles: A review. *Advances in Space Research*, *61*(1), 1–44.

Pilipenko, V. A., Fedorov, E. N., Xu, Z., Hartinger, M. D., Engebretson, M. J., & Edwards, T. R. (2020). Incidence of alfvenic sc pulse onto the conjugate ionospheres. *Journal of Geophysical Research: Space Physics*, *125*, e2019JA027397. https://doi.org/10.1029/2019JA027397

Pirjola, R. (2002). Review on the calculation of surface electric and magnetic fields and of geomagnetically induced currents in ground-based technological systems. *Surveys in Geophysics*, *23*(1), 71–90.

Richter, A. K., Hsieh, K. C., Luttrell, A. H., Marsch, E., & Schwenn, R. (1985). Review of interplanetary shock phenomena near and within 1 AU. In B. T. Tsurutani & R. G. Stone (Eds.), *Collisionless shocks in the heliosphere: Reviews of current research, Geophysical Monograph Series* (Vol. 35, pp. 33–50). Washington, DC: American Geophysical Union.

Rudd, J. T., Oliveira, D. M., Bhaskar, A., & Halford, A. J. (2019). How do interplanetary shock impact angles control the size of the geoeffective magnetosphere? *Advances in Space Research*, *63*(1), 317–326.

Samsonov, A. A. (2011). Propagation of inclined interplanetary shock through the magnetosheath. *Journal of Atmospheric and Solar-Terrestrial Physics*, *73*(1), 1–9.

Samsonov, A. A., Sergeev, V. A., Kuznetsova, M. M., & Sibeck, D. G. (2015). Asymmetric magnetospheric compressions and expansions in response to impact of inclined interplanetary shock. *Geophysical Research Letters*, *42*, 4716–4722. https://doi.org/10.1002/2015GL064294

Selvakumaran, R., Veenadhari, B., Ebihara, Y., Kumar, S., & Prasad, D. S. V. V. D. (2017). The role of interplanetary shock orientation on SC/SI rise time and geoeffectiveness. *Advances in Space Research*, *59*(5), 1425–1434.

Shi, Y., Oliveira, D. M., Knipp, D. J., Zesta, E., Matsuo, T., & Anderson, B. (2019). Effects of nearly frontal and highly inclined interplanetary shocks on high-latitude field-aligned currents (FACs). *Space Weather*, *17*, 1659–1673. https://doi.org/10.1029/2019SW002367

Smith, E. J., Slavin, J. A., Zwickl, R. D., & Bame, S. J. (1986). Shocks and storm sudden commencements. In Y. Kamide & J. A. Slavin (Eds.), *Solar wind and magnetosphere coupling* (pp. 345). Tokyo, Japan: Terra Scientific.

Takeuchi, T., Russell, C. T., & Araki, T. (2002). Effect of the orientation of interplanetary shock on the geomagnetic sudden commencement. *Journal of Geophysical Research*, *107*(A12), SMP 6–1–SMP 6–10.

Tsurutani, B. T., Lakhina, G. S., Verkhoglyadova, O. P., Gonzalez, W. D., Echer, E., & Guarnieri, F. L. (2011). A review of interplanetary discontinuities and their geomagnetic effects. *Journal of Atmospheric and Solar-Terrestrial Physics*, *73*(1), 5–19.

Viljanen, A. (1998). Relation of geomagnetically induced currents and local geomagnetic variations. *IEEE Transactions on Power Delivery*, *13*(4), 1285–1290.

Wang, C., Li, C. X., Huang, Z. H., & Richardson, J. D. (2006). Effect of interplanetary shock strengths and orientations on storm sudden commencement rise times. *Geophysical Research Letters*, *33*, L14104. https://doi.org/10.1029/2006GL025966

Xu, Z., Hartinger, M. D., Clauer, C. R., Peek, T., & Behlke, R. (2017). A comparison of the ground magnetic responses during the 2013 and 2015 St. Patrick's Day geomagnetic storms. *Journal of Geophysical Research: Space Physics*, *122*, 4023–4036. https://doi.org/10.1002/2016JA023338

Yue, C., & Zong, Q. (2011). Solar wind parameters and geomagnetic indices for four different interplanetary shock/ICME structures. *Journal of Geophysical Research*, *116*, A12201. https://doi.org/10.1029/2011JA017013

Zhang, J. J., Wang, C., Sun, T. R., & Liu, Y. D. (2016). Risk assessment of the extreme interplanetary shock of 23 July 2012 on low-latitude power networks. *Space Weather*, *14*, 259–270. https://doi.org/10.1002/2015SW001347

Zhang, J. J., Wang, C., Sun, T. R., Liu, C. M., & Wang, K. R. (2015). GIC due to storm sudden commencement in low-latitude high-voltage power network in China: Observation and simulation. *Space Weather*, *13*, 643–655. https://doi.org/10.1002/2015SW001263

Zhou, X., & Tsurutani, B. T. (2001). Interplanetary shock triggering of nightside geomagnetic activity: Substorms, pseudobreakups, and quiescent events. *Journal of Geophysical Research*, *106*(A9), 18,957–18,967.